Coupled-mode calculation with the *R*-matrix propagator for the dispersion of surface waves on a truncated photonic crystal

J. Merle Elson and P. Tran
Research and Technology Division, Naval Air Warfare Center Weapons Division, China Lake, California 93555-6001
(Received 11 January 1996)

We describe a modal expansion method with an *R*-matrix propagation algorithm that can be applied to calculate the dispersion of surface and guided waves supported by a finite thickness photonic crystal. Easy to implement, the *R* matrix has the advantage of inherent numerical stability and allows photonic crystals of complex structure, which are many waves in thickness to be analyzed. This method is also computationally simpler that the supercell method when looking for surface modes. It can also be applied to many other dispersion problems including multilayer gratings and waveguides with internal structure. We apply this method to calculate dispersion of surface waves supported by a slablike photonic crystal structure, which consists of several rows of an infinitely periodic array of square dielectric cylinders. In the bulk, the periodic array has a photonic band gap and for the finite thickness structure, we calculate dispersion of surface waves that propagate along the boundaries at frequencies within the band gap. We vary the thickness of the cylinders in the outer layer and calculate the change in dispersion. When the overall thickness of the photonic slab is decreased, coupling and splitting between surface modes at each interface is observed. [S0163-1829(96)03727-7]

I. INTRODUCTION

Recently, the authors have described calculation techniques that utilize an *R*-matrix propagation algorithm, as applied to diffraction from deep sinusoidal gratings and dispersion in photonic media of infinite extent.[1,2] In Ref. 1, we considered an approach similar to that presented here except that modal expansion solutions were obtained in a Fourier space representation. In Ref. 2, we considered an approach based on a numerical integration of Maxwell's equations represented in a frequency domain finite-difference approximation. The present method also uses a finite-difference approximation to Maxwell's equations but solutions are obtained as modal expansions in real space. In Sec. II, we describe in detail the approach we use here to calculate the dispersion of surface waves that propagate along the interface(s) of a finite thickness photonic structure.

The instability of the *T* matrix due to evanescent waves is well known. The *T* matrix generally has elements dependent upon exponential terms such as $\exp(\pm\alpha\Delta z)$ where Δz is the distance between two interfaces. When the exponential term is evanescent (α real), numerical instability arises due to exponential overflow and underflow. The *R*-matrix propagation method has proven to be much more numerically stable than *T*-matrix propagation schemes as it seeks a matrix *R* that relates the derivative of a quantity (for the case considered here, it is the magnetic field) to the quantity itself (electric field). For this reason, the elements of the *R* matrix tend to be proportional to $\pm\alpha\Delta z$. This is especially important when the structure under consideration is many wavelengths thick. In addition to the original application of this method in chemical physics,[3] several authors have recently applied the *R*-matrix approach to various problems of electromagnetic theory.[1,2,4–6]

A photonic crystal offers the possibility of controlling the flow of photons in a way analogous to an electronic crystal and electrons. Many applications of photonic crystals have been suggested. One such application is to make a high-*Q* laser cavity by putting defects into a photonic crystal. In addition to a regular defect mode, there is the possibility of surface modes when the crystal is cleaved. Meade *et al.*[7] were the first to study and discuss the importance of surface modes of truncated photonic crystals in the operation of high-*Q* laser cavities. To calculate such modes they used a supercell method to simulate a semi-infinite crystal. The supercell method is the standard technique to study defect modes, but it is quite demanding on computer resources as one needs to keep more plane waves in the expansion to reflect the larger unit cell. The *R*-matrix method we describe here provides a way to calculate surface modes without this additional burden.

II. THEORETICAL APPROACH

We assume the photonic crystal structure is infinitely periodic in the $\hat{\mathbf{x}}$ direction, uniform in the $\hat{\mathbf{y}}$ direction, and of finite thickness in the $\hat{\mathbf{z}}$ direction. However, the following discussion assumes the structure is not necessarily independent of the *y* coordinate. The substrate and superstrate regions are homogeneous with permittivities ε_t and ε_r, respectively. The photonic crystal structure is inhomogeneous (piecewise homogeneous) and is described by a spatially variable permittivity $\varepsilon(\mathbf{r})$ where $\mathbf{r}=(x,y,z)$. The basic photonic structure considered here, along with associated nomenclature, is shown in Fig. 1. Figure 1 shows three rows of cylinders with the middle cylinders having a square cross section and the outer cylinders, having been truncated in the *z* direction, having a rectangular cross section. In Sec. III, we consider the example shown in Fig. 1 and also the case where there are six rows of square cylinders between the truncated outer rows. The square cylinders have cross section

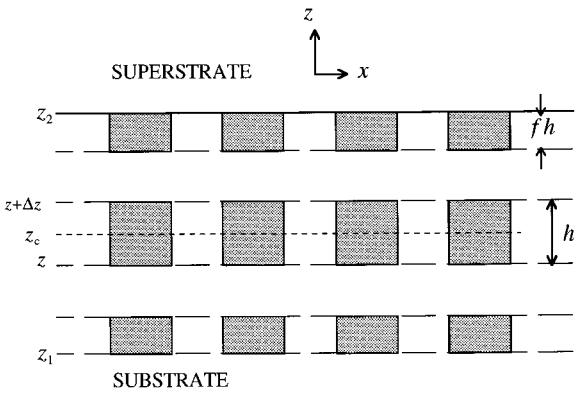

FIG. 1. Schematic of photonic structure of rows of dielectric cylinders. The middle row consists of square cylinders of dimension $h=0.74$ mm. The outer rows are truncated in the z direction by fraction f. The cylinders are infinitely periodic in the x direction with period $a=1.87$ mm. The long dashed line indicates sublayer divisions. The dotted line shows an example of the center z coordinate z_c of the sublayer bounded from z to $z+\Delta z$. Some of the numerical results based on six rows are square cylinders between the truncated outer rows.

of dimension h and the outer cylinders have dimension h by fh where $f<1$. This system has three distinct regions: the homogeneous substrate, the photonic crystal, and the homogeneous superstrate. The fields in the two homogeneous regions are just plane waves and are known. If we can obtain the field in the photonic crystal, we can match boundary conditions and solve for surface modes. The solution to the general Maxwell's equations can be obtained if there is no z dependence in the dielectric permittivity (the homogeneous system is a special case of this). Therefore, we further divide the photonic crystal into sublayers such that within each sublayer, we can approximate with a z-independent permittivity. Modal solutions within each sublayer can then be obtained. Since the cylinders are of square or rectangular cross section, this photonic structure is a simple geometry to obtain sublayers where the permittivity is independent of the z coordinate. In Fig. 1, the sublayer divisions are shown by the long-dashed lines. For circular or more complicated cross sections, more sublayers can be used to approximate the actual shape. In any case, the sublayer modal solutions are used to obtain an r matrix that relates the magnetic fields at the boundaries of the sublayer to the electric fields. From the boundary conditions between sublayers, we obtain a recursive formula for adding two r matrices. The global R matrix is obtained by recursion through successive sublayers and this matrix relates the fields at the boundaries $z=z_1$ and $z=z_2$ of the whole finite thickness photonic structure.

A. Sublayer modal solution

The procedure outlined below parallels that given in Ref. 1, except that this work is done in real space whereas the method of Ref. 1 is based on a Fourier-space representation. The reason for going to a real-space representation is that the Fourier representation can have convergence difficulties for sharp discontinuities in the dielectric permittivity $\varepsilon(\mathbf{r})$. We now obtain the modal expansion solution for a sublayer of the modulation region bounded between $z\rightarrow z+\Delta z$. The sublayer has thickness Δz, which need not be small compared to the wavelength. Within a sublayer, the permittivity can have x dependence, but we require no z variation in the permittivity within a sublayer. Because of this we can in general evaluate the permittivity at the z coordinate z_c where $z_c=z+\Delta z/2$ is the center of the sublayer. However, since we have chosen a square or rectangular cross section, the permittivity is the same for any value of z within the sublayer and this is a special case of the more general problem. We now discretize the x coordinate over one period a into n_x points separated by $\Delta x=a/n_x$. From the two Maxwell equations $\nabla\times\mathbf{E}(\mathbf{r})=i(\omega/c)\mathbf{H}(\mathbf{r})$ and $\nabla\times\mathbf{H}(\mathbf{r})=-i(\omega/c)\varepsilon(\mathbf{r})\mathbf{E}(\mathbf{r})$, we eliminate the z component of the fields and arrive at a set of coupled equations:

$$\frac{\partial E_x(x,z)}{\partial z}=\frac{i\omega}{c}H_y(x,z)+\frac{ic}{\omega(\Delta x)^2}\times\left\{\frac{H_y(x+\Delta x,z)-H_y(x,z)}{\varepsilon(x+\Delta x/2,z_c)}+\frac{H_y(x-\Delta x,z)-H_y(x,z)}{\varepsilon(x-\Delta x/2,z_c)}\right\},\tag{1a}$$

$$\frac{\partial E_y(x,z)}{\partial z}=-\frac{i\omega}{c}H_x(x,z),\tag{1b}$$

$$\frac{\partial H_x(x,z)}{\partial z}=-\frac{i\omega}{c}\varepsilon(x,z_c)E_y(x,z)+\frac{ic}{\omega(\Delta x)^2}\times\{2E_y(x,z)-E_y(x+\Delta x,z)-E_y(x-\Delta x,z)\},\tag{1c}$$

$$\frac{\partial H_t(x,z)}{\partial z}=\frac{i\omega}{c}\varepsilon(x,z_c)E_x(x,z).\tag{1d}$$

Note that we use a finite-difference approximation for the x derivative in Eq. (1). These coupled differential equations have coefficients that are independent of z for a given sublayer. When we include the set of all n_x discrete x coordinates, denoted by $\mathbf{X}$, Eq. (1) may be written in matrix form as

$$\frac{\partial\mathbf{A}(\mathbf{X},z)}{\partial z}=\mathbf{M}(\mathbf{X},z_c)\mathbf{A}(\mathbf{X},z),\tag{2}$$

where

$$\mathbf{A}(\mathbf{X},z)=\begin{pmatrix}E_x(\mathbf{X},z)\\E_y(\mathbf{X},z)\\H_x(\mathbf{X},z)\\H_y(\mathbf{X},z)\end{pmatrix}=\begin{pmatrix}\tilde{\mathbf{E}}(\mathbf{X},z)\\\tilde{\mathbf{H}}(\mathbf{X},z)\end{pmatrix}.\tag{3}$$

The $\tilde{\mathbf{E}}$ and $\tilde{\mathbf{H}}$ represent abbreviated column vectors as

$$\tilde{\mathbf{E}}=\begin{pmatrix}E_x\\E_y\end{pmatrix},\quad\tilde{\mathbf{H}}=\begin{pmatrix}H_x\\H_y\end{pmatrix}.\tag{4}$$

Since $\mathbf{M}$ is independent of z within the sublayer, the solution is straightforward by diagonalization of $\mathbf{M}$:

$$\begin{pmatrix}\tilde{\mathbf{E}}(\mathbf{X},z)\\ \tilde{\mathbf{H}}(\mathbf{X},z)\end{pmatrix}=\mathbf{S}(\mathbf{X},z_c)\mathbf{e}^{\Lambda z}\mathbf{C}=\begin{pmatrix}\mathbf{S}_{11} & \mathbf{S}_{12}\\ \mathbf{S}_{21} & \mathbf{S}_{22}\end{pmatrix}\begin{pmatrix}\mathbf{e}^{\lambda z} & \mathbf{0}\\ \mathbf{0} & \mathbf{e}^{-\lambda z}\end{pmatrix}\begin{pmatrix}\mathbf{C}_+\\ \mathbf{C}_-\end{pmatrix}. \tag{5}$$

The square matrix $\mathbf{S}(\mathbf{X},z_c)$ has columns that are the eigenvectors of $\mathbf{M}(\mathbf{X},z_c)$ and $\mathbf{e}^{\Lambda z}$ is a diagonal matrix of exponential terms with Λ representing the set of eigenvalues associated with $\mathbf{M}(\mathbf{X},z_c)$. $\mathbf{C}$ is a column vector of constants. In the right-hand side of Eq. (5), the matrices and column vector have been sectored. The columns of eigenvectors are subdivided into four matrices and the set of eigenvalues Λ are divided into two sets, denoted by $+\lambda$ and $-\lambda$, such that the members of one set are the opposite sign of the other. Note that this division is for convenience only. Solutions given by Eq. (5) apply to a given sublayer and to complete the problem, the solutions for all sublayers are combined by a recursive algorithm, as shown below.

B. Recursive *R*-matrix algorithm

In this section, we describe the calculation of the sublayer r matrix from the modal solution and the recursion formula for the global R matrix. The sublayer r matrix is defined as

$$\begin{pmatrix}\tilde{\mathbf{E}}(\mathbf{X},z)\\ \tilde{\mathbf{E}}(\mathbf{X},z+\Delta z)\end{pmatrix}=\mathbf{r}(\Delta z)\begin{pmatrix}\tilde{\mathbf{H}}(\mathbf{X},z)\\ \tilde{\mathbf{H}}(\mathbf{X},z+\Delta z)\end{pmatrix}, \tag{6}$$

where Δz is the thickness of a sublayer. The r matrix relates the electric fields to the corresponding magnetic fields at the sublayer boundaries. This matrix is dependent on the thickness of the sublayer and the eigenvectors and eigenvalues of the matrix M. Using the defining relation given in Eq. (6) with Eq. (5) we find that

$$\mathbf{r}(\Delta z)=\begin{pmatrix}\mathbf{r}_{11}(\Delta z) & \mathbf{r}_{12}(\Delta z)\\ \mathbf{r}_{21}(\Delta z) & \mathbf{r}_{22}(\Delta z)\end{pmatrix}=\begin{pmatrix}\mathbf{S}_{11} & \mathbf{S}_{12}\\ \mathbf{S}_{11}\mathbf{e}^{\lambda\Delta z} & \mathbf{S}_{12}\mathbf{e}^{-\lambda\Delta z}\end{pmatrix}\times\begin{pmatrix}\mathbf{S}_{21} & \mathbf{S}_{22}\\ \mathbf{S}_{21}\mathbf{e}^{\lambda\Delta z} & \mathbf{S}_{22}\mathbf{e}^{-\lambda\Delta z}\end{pmatrix}^{-1}. \tag{7}$$

We also assume that a relation similar to Eq. (6) exists, which includes an arbitrary number of sublayers ranging from $z=z_1$ to $z=z_2$ and this defines the global matrix R as

$$\begin{pmatrix}\tilde{\mathbf{E}}(\mathbf{X},z_1)\\ \tilde{\mathbf{E}}(\mathbf{X},z_2)\end{pmatrix}=\mathbf{R}(z_2-z_1)\begin{pmatrix}\tilde{\mathbf{H}}(\mathbf{X},z_1)\\ \tilde{\mathbf{H}}(\mathbf{X},z_2)\end{pmatrix}, \tag{8a}$$

where

$$\mathbf{R}(z_2-z_1)=\begin{pmatrix}\mathbf{R}_{11}(z_2-z_1) & \mathbf{R}_{12}(z_2-z_1)\\ \mathbf{R}_{21}(z_2-z_1) & \mathbf{R}_{22}(z_2-z_1)\end{pmatrix}. \tag{8b}$$

Using Eqs. (6), (7), and (8) along with the continuity of the column vectors in Eq. (5), we obtain the following recursive relationships:

$$\mathbf{R}_{11}(z_2-z_1)=\mathbf{R}_{11}(z_2-\Delta z-z_1)+\mathbf{R}_{12}(z_2-\Delta z-z_1)\times[\mathbf{r}_{11}(\Delta z)-\mathbf{R}_{22}(z_2-\Delta z-z_1)]^{-1}\times\mathbf{R}_{21}(z_2-\Delta z-z_1), \tag{9a}$$

$$\mathbf{R}_{12}(z_2-z_1)=-\mathbf{R}_{12}(z_2-\Delta z-z_1)[\mathbf{r}_{11}(\Delta z)-\mathbf{R}_{22}(z_2-\Delta z-z_1)]^{-1}\mathbf{r}_{12}(\Delta z), \tag{9b}$$

$$\mathbf{R}_{21}(z_2-z_1)=\mathbf{r}_{21}(\Delta z)[\mathbf{r}_{11}(\Delta z)-\mathbf{R}_{22}(z_2-\Delta z-z_1)]^{-1}\times\mathbf{R}_{21}(z_2-\Delta z-z_1), \tag{9c}$$

$$\mathbf{R}_{22}(z_2-z_1)=\mathbf{r}_{22}(\Delta z)-\mathbf{r}_{21}(\Delta z)[\mathbf{r}_{11}(\Delta z)-\mathbf{R}_{22}(z_2-\Delta z-z_1)]^{-1}\mathbf{r}_{12}(\Delta z). \tag{9d}$$

From Eqs. (6) and (8a), we see that we can set $z_2=z_1+\Delta z$ and initialize the global R matrix by $\mathbf{R}(\Delta z)=\mathbf{r}(\Delta z)$.

The R matrix can be calculated from Eq. (9) for any structure of interest by recursively adding n_z successive sublayers where the r matrix is calculated for each sublayer. It is important to point out that the R matrix depends *only* on the thickness z_2-z_1 of the region. Because of this, we observe that repeating inhomogeneous regions each of thickness z_2-z_1 can also be added by recursion, whole regions at a time. This is accomplished by using Eq. (9) to calculate $\mathbf{R}(z_2-z_1)$ for a given structure. With this, we return to Eq. (9), set $\mathbf{R}(z_2-z_1)\equiv\mathbf{r}(\Delta z)$ and apply $N-1$ times, which yields $\mathbf{R}_N(N[z_2-z_1])$ for a structure that has N identical regions. This is very significant in terms of potential computational efficiency and experience has shown that the procedure is numerically stable.

C. Calculation of surface and guided modes

Having found the $\mathbf{R}$ matrix for a given structure, we match boundary conditions to include the superstrate and substrate media. This yields

$$\begin{pmatrix}\tilde{\mathbf{E}}^t(\mathbf{X},z_1)\\ \tilde{\mathbf{E}}^r(\mathbf{X},z_2)\end{pmatrix}=\mathbf{R}(z_2-z_1)\begin{pmatrix}\tilde{\mathbf{H}}^t(\mathbf{X},z_1)\\ \tilde{\mathbf{H}}^r(\mathbf{X},z_2)\end{pmatrix}. \tag{10}$$

Since the superstrate (denoted by r) and substrate (denoted by t) are homogeneous, the $\tilde{\mathbf{E}}$ and $\tilde{\mathbf{H}}$ fields have a simple relation in Fourier space,

$$\tilde{\mathbf{H}}^j(\mathbf{K},z)=\mathbf{Z}^j(\mathbf{K},p_j)\tilde{\mathbf{E}}^j(\mathbf{K},z), \tag{11}$$

where $j=r$ or t and

$$\mathbf{Z}^j(\mathbf{K},p_j)=\begin{pmatrix}-\dfrac{K_xK_y}{(\omega/c)p_j} & -\dfrac{p_j^2+K_y^2}{(\omega/c)p_j}\\ \dfrac{p_j^2+K_x^2}{(\omega/c)p_j} & \dfrac{K_xK_y}{(\omega/c)p_j}\end{pmatrix}, \tag{12}$$

with $p_j=\sqrt{(\omega/c)^2\varepsilon_j-K^2}$, $K=|\mathbf{K}|$, $\mathbf{K}=(K_x,K_y)$, and ε_j is the permittivity of the medium denoted by j. The four quadrants of Eq. (13) represent diagonal matrices. To get a real-space analog of Eq. (11), we just apply a Fourier transform to Eq. (11),

$$\tilde{\mathbf{E}}^j(\mathbf{X},z)=\mathbf{F}(\mathbf{X},\mathbf{K})\tilde{\mathbf{E}}^j(\mathbf{K},z),\quad \tilde{\mathbf{H}}^j(\mathbf{X},z)=\mathbf{F}(\mathbf{X},\mathbf{K})\tilde{\mathbf{H}}^j(\mathbf{K},z), \tag{13}$$

where $\mathbf{F}(\mathbf{X},\mathbf{K})$ is a square Fourier transform matrix.

Using Eqs. (11) and (13) in Eq. (10) yields the homogeneous matrix equation

$$\begin{pmatrix}\mathbf{I}-\overline{\mathbf{R}}_{11}\mathbf{Z}^t(\mathbf{K},-p_t) & -\overline{\mathbf{R}}_{12}\mathbf{Z}^r(\mathbf{K},p_r)\\ -\overline{\mathbf{R}}_{21}\mathbf{Z}^t(\mathbf{K},-p_t) & \mathbf{I}-\overline{\mathbf{R}}_{22}\mathbf{Z}^r(\mathbf{K},p_r)\end{pmatrix}\begin{pmatrix}\tilde{\mathbf{E}}^t(\mathbf{K},z_1)\\ \tilde{\mathbf{E}}^r(\mathbf{K},z_2)\end{pmatrix}=\mathbf{0}, \tag{14}$$

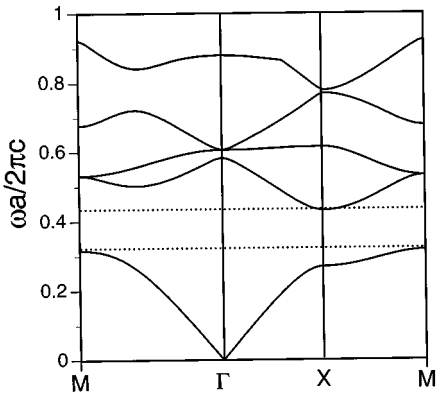

FIG. 2. Photonic band structure of an infinitely periodic square array of dielectric cylinders with square cross section. The polarization is parallel to the axes of the cylinders and the propagation is perpendicular to the axes of the cylinders. The cylinders have side dimension $h=0.74$ mm, period $a=1.87$ mm, and permittivity (9,0). The space between cylinders is vacuum. Note the complete band gap between 0.317 and 0.431.

where $\mathbf{I}$ is the identity matrix and $\overline{\mathbf{R}}=\mathbf{F}^{-1}\mathbf{R}\mathbf{F}$. Equation (14) may also be written in the form of an eigenvalue equation as

$$\begin{pmatrix} \overline{\mathbf{R}}_{11}\mathbf{Z}^t(\mathbf{K},-p_t) & \overline{\mathbf{R}}_{12}(\mathbf{K},p_r) \\ \overline{\mathbf{R}}_{21}\mathbf{Z}^t(\mathbf{K},-p_t) & \overline{\mathbf{R}}_{22}\mathbf{Z}^r(\mathbf{K},p_r) \end{pmatrix} \begin{pmatrix} \tilde{\mathbf{E}}^t(\mathbf{K},z_1) \\ \tilde{\mathbf{E}}^r(\mathbf{K},z_2) \end{pmatrix} = \begin{pmatrix} \tilde{\mathbf{E}}^t(\mathbf{K},z_1) \\ \tilde{\mathbf{E}}^r(\mathbf{K},z_2) \end{pmatrix}. \tag{15}$$

Either Eq. (14) or (15) can be used to obtain the band structure associated with infinite (bulk) or truncated photonic crystals. In Eq. (14), zeros in the matrix determinant yield $(\mathbf{K},\omega)$ solutions for surface and guided modes. In Eq. (15), unit eigenvalues of the matrix yield similar solutions with the associated eigenvector.

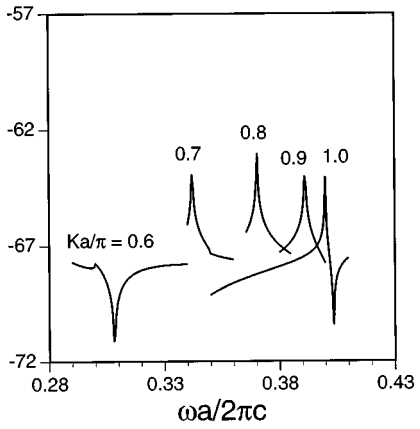

FIG. 3. Plot of $\ln(|D|^{-2})$ vs frequency for several wave numbers. For frequencies in the band gap shown in Fig. 2, resonance peaks are clearly seen for normalized wave numbers 0.7 to 1.0. No resonance is seen for 0.6 because we have crossed the lightline $K=\omega/c$. These data are for cylinders in the outer rows with $f=0.3$ and for six rows of square cylinders in between the outer rows.

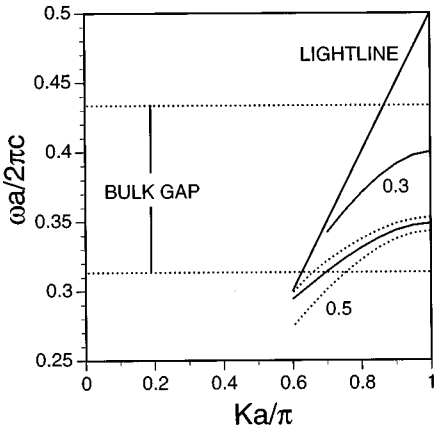

FIG. 4. Surface mode dispersion for two values of surface truncation and number of rows of cylinders. The bulk gap, as shown in Fig. 2, is indicated between the horizontal dotted lines. The outer rows of cylinders have thickness fh where $f=0.3$ and 0.5. The solid dispersion curves are for six rows of square cylinders between the truncated outer rows. For $f=0.5$, the dotted dispersion curves, which are for one row of square cylinders between the outer layers, represent splitting from the corresponding solid curve. This is a result of modes at each interface coupling because of their close proximity.

III. NUMERICAL RESULTS

We examine here the case of polarization parallel to the cylinder axis. We do not consider polarization perpendicular to the rods because the photonic band gap is quite small.[2] For polarization parallel to the axes of the rods and for propagation perpendicular to the axes of the rods, the bulk photonic crystal has a complete band gap for the approximate normalized frequency range $0.317\leqslant\omega a/2\pi c\leqslant 0.431$. The bulk band structure, calculated using the plane-wave expansion of Plihal *et al.*[8] is shown in Fig. 2. This band structure is for an infinitely periodic square lattice of dielectric cylinders with square cross section. The cylinders have side dimension $h=0.74$ mm, are periodic with period $a=1.87$ mm, and have permittivity (9,0). The space between cylinders is vacuum. Since bulk photon modes cannot propagate within the band gap, we look for mode solutions within this frequency range that are also evanescent into the homogeneous media: $K>(\omega/c)\varepsilon_j$ $(j=r$ or $t)$. We choose the homogeneous media to be vacuum $\varepsilon_j=(1,0)$. Under these conditions, modes cannot propagate in either the crystal lattice or into the homogeneous regions. Thus, the mode solution, if any, is constrained to propagate along the surface of the finite thickness truncated photonic crystal.

We consider two values for the outer row thickness of the rectangular rods, which are $f=0.3$ and 0.5. We also consider two values for the number of rows of square rods in between the outer rows of rectangular rods. We consider one row and six rows where Fig. 1 shows one row of square rods. For the case with only one row of rods, the surface modes are strongly coupled and splitting is evident.

The surface mode dispersion is obtained by either of the two methods discussed at the end of Sec. II. When using Eq. (14), we fix the wave vector K and vary ω until a zero in the determinant is found. Because the determinant is complex in general, we choose to look at $|D|^{-2}$, where D is the deter-

minant, as a function of frequency. The surface mode would then appear as a peak in the ω scan. In Fig. 3, we show the plot of $\log_{10}(|D|^{-2})$ versus ω for five values of K for the case $f=0.3$. Note that for $Ka/\pi=0.6$, there is no resonance as we have passed through the lightline $K=\omega/c$. The dispersion curve for the surface mode is shown in Fig. 4. Also shown in Fig. 4 is the dispersion for the case $f=0.5$. For this case we show the result for both 1 and 6 rows of rods between the outer rows. The case of 1 row of rods in between (dotted lines) shows splitting in the surface mode as the modes at the two interfaces couple to each other.

One disadvantage of using Eq. (14) is lack of information on the characteristics of the surface modes. In addition, if two mode solutions are close together as can occur when splitting is present, their two peaks may not be resolved and appear as only one peak. Using Eq. (15) provides an alternate approach where the wave vector K is fixed and ω is varied until an eigenvalue of 1 is found. The associated eigenvector yields mode characteristics such as polarization and spatial intensity distribution at the surface of the photonic crystal. Also, unit eigenvalues can be found to find surface modes that are close in frequency and yet their resonance peaks appear as one.

Calculation of guided modes is quite straightforward by either of the methods discussed above. We simply choose $K>\omega/c$ to assure evanescent fields in the homogeneous regions and choose frequency ω within band-gap frequencies.

In conclusion, we have described an *R*-matrix propagation technique for the computation of surface and guided modes supported by truncated photonic crystals that is computationally simpler than the supercell method.

ACKNOWLEDGMENTS

This work was supported in part by a grant of HPC time from the DoD HPC Center U.S. Army Corp of Engineers Waterways Experiment Station (Cray Research C-916 and Y-MP). Support for the authors was provided by Navy In-House Independent Research funds.

[1] J. M. Elson and P. Tran, J. Opt. Soc. Am. A **12**, l765 (l995).

[2] J. M. Elson and P. Tran, in *Photonic Band Gap Materials*, Vol. 315, *NATO Advanced Study Institute Series E: Applied Sciences*, edited by C. M. Soukoulis (Kluwer, Dordrecht, 1996), p. 341.

[3] D. J. Zvijac and J. C. Light, Chem. Phys. **12**, 237 (l976); J. C. Light and R. B. Walker, J. Chem. Phys. **65**, 4272 (1976).

[4] L. F. DeSandre and J. M. Elson, J. Opt. Soc. Am. A **8**, 763 (1991).

[5] L. Li, J. Opt. Soc. Am. A **10**, 2581 (1993).

[6] F. Montiel and M. Neviere, J. Opt. Soc. Am. A **11**, 3241 (1994).

[7] R. D. Meade, K. D. Brommer, A. M. Rappe, and J. D. Joannopoulos, Phys. Rev. B **44**, 10 961 (1991).

[8] M. Plihal, A. Shambrook, A. A. Maradudin, and P. Sheng, Opt. Commun. **80**, 199 (1991).